Icarus xxx (2011) xxx–xxx

Contents lists available at ScienceDirect

Icarus

journal homepage: www.elsevier.com/locate/icarus

In search of water vapor on Jupiter: Laboratory measurements of the microwave properties of water vapor under simulated jovian conditions

Bryan M. Karpowicz [a,*], Paul G. Steffes [b,1]

[a] School of Earth and Atmospheric Sciences, Georgia Institute of Technology, Atlanta, GA 30332-0250, United States
[b] School of Electrical and Computer Engineering, Georgia Institute of Technology, Atlanta, GA 30332-0250, United States

ARTICLE INFO

Article history:
Received 20 June 2010
Revised 21 November 2010
Accepted 23 November 2010
Available online xxxx

Keywords:
Jupiter, Atmosphere
Saturn, Atmosphere
Radio observations
Atmospheres, Composition
Spectroscopy

ABSTRACT

Detection and measurement of atmospheric water vapor in the deep jovian atmosphere using microwave radiometry has been discussed extensively by Janssen et al. (Janssen, M.A., Hofstadter, M.D., Gulkis, S., Ingersoll, A.P., Allison, M., Bolton, S.J., Levin, S.M., Kamp, L.W. [2005]. Icarus 173 (2), 447–453.) and de Pater et al. (de Pater, I., Deboer, D., Marley, M., Freedman, R., Young, R. [2005]. Icarus 173 (2), 425–447). The NASA Juno mission will include a six-channel microwave radiometer system (MWR) operating in the 1.3–50 cm wavelength range in order to retrieve water vapor abundances from the microwave signature of Jupiter (see, e.g., Matousek, S. [2005]. The Juno new frontiers mission. Tech. Rep. IAC-05-A3.2.A.04, California Institute of Technology). In order to accurately interpret data from such observations, nearly 2000 laboratory measurements of the microwave opacity of H_2O vapor in a H_2/He atmosphere have been conducted in the 5–21 cm wavelength range (1.4–6 GHz) at pressures from 30 mbars to 101 bars and at temperatures from 330 to 525 K. The mole fraction of H_2O (at maximum pressure) ranged from 0.19% to 3.6% with some additional measurements of pure H_2O. These results have enabled development of the first model for the opacity of gaseous H_2O in a H_2/He atmosphere under jovian conditions developed from actual laboratory data. The new model is based on a terrestrial model of Rosenkranz et al. (Rosenkranz, P.W. [1998]. Radio Science 33, 919–928), with substantial modifications to reflect the effects of jovian conditions. The new model for water vapor opacity dramatically outperforms previous models and will provide reliable results for temperatures from 300 to 525 K, at pressures up to 100 bars and at frequencies up to 6 GHz. These results will significantly reduce the uncertainties in the retrieval of jovian atmospheric water vapor abundances from the microwave radiometric measurements from the upcoming NASA Juno mission, as well as provide a clearer understanding of the role deep atmospheric water vapor may play in the decimeter-wavelength spectrum of Saturn.

1. Introduction

Initial modeling studies have been performed which show that it is possible to retrieve water vapor abundance in Jupiter's deep atmosphere using a multi-channel radiometer as proposed for the NASA Juno mission (Janssen et al., 2005; Matousek, 2005), but there are a number of factors which limit the accuracy of this approach (de Pater et al., 2005). The most critical of these is the knowledge of the microwave absorption properties of water vapor under jovian conditions. Previous laboratory measurements of the microwave opacity of water vapor under pressures and temperatures representative of Jupiter have been conducted in a nitrogen atmosphere (Ho et al., 1966), but not in a hydrogen–helium atmosphere. While models for water vapor absorption have been extrapolated to a hydrogen–helium atmosphere (Goodman (1969), and the DeBoer model, which appears in de Pater et al. (2005)), far more accurate measurements are necessary to accurately retrieve the jovian water vapor abundance (de Pater et al., 2005).

In this laboratory measurement campaign, nearly 2000 laboratory measurements of the microwave opacity of H_2O vapor in a H_2/He atmosphere have been conducted in the 5–21 cm wavelength range (1.4–6 GHz) at pressures from 30 mbars to 101 bars and at temperatures from 330 to 525 K. The mole fraction of H_2O (at maximum pressure) ranged from 0.19% to 3.6% with some additional measurements of pure H_2O. These results have enabled development of the first model for the opacity of gaseous H_2O in a H_2/He atmosphere under jovian conditions developed from laboratory data of H_2/He/H_2O mixtures. The new model is based on a terrestrial model of Rosenkranz (1998), with substantial modifications to reflect the effects of jovian conditions. The new model for water

* Corresponding author. Fax: +1 781 761 2299.
E-mail addresses: bkarpowi@aer.com (B.M. Karpowicz), steffes@gatech.edu (P.G. Steffes).
[1] Fax: +1 781 761 2299.

0019-1035/$ - see front matter © 2011 Elsevier Inc. All rights reserved.
doi:10.1016/j.icarus.2010.11.035

vapor opacity dramatically outperforms previous models and will provide reliable results for temperatures from 330 to 525 K, at pressures up to 100 bars and at frequencies between 1.4 and 6 GHz. The new formalism developed in this work outperforms jovian models such as the DeBoer model as it appears in de Pater et al. (2005), and the Goodman (1969) model, owing to the fact that neither model considers the well established existence of continuum water vapor absorption (see, e.g. Rosenkranz, 1998; Payne et al., 2008). By ignoring the continuum effect both the DeBoer and Goodman models over-estimate the opacity contribution from the foreign gas (H_2 and He), and not enough opacity is attributed to the amount of water vapor present. Also in both the DeBoer and Goodman (1969) models, the contributions from absorption lines are overestimated as each model attempts to attribute absorption from water vapor lines alone.

2. Measurement theory

The method used to measure the microwave absorptivity of a gas is based on the lessening in the quality factor (Q) of a resonant mode of a cylindrical cavity in the presence of a lossy gas. This technique involves monitoring the changes in Q of different resonances of a cavity resonator in order to determine the refractive index and the absorption coefficient of an introduced gas or gas mixture (at those resonant frequencies). Described at length by Hanley and Steffes (2007), it has been successfully utilized for over one half of a century (i.e., Bleaney and Loubser, 1950). The cavity resonator technique for measuring refractivity based on frequency shifts has had similar effectiveness, and is also described by Hanley and Steffes (2007). The cylindrical cavity resonator used in these experiments consists of a section of cylindrical waveguide capped at both ends, with resonant modes resulting from various standing-wave patterns. The quality factor of a resonance within a microwave resonator is defined by

$$Q^m_{resonance} = \frac{2\pi f_o \times \text{Energy stored}}{\text{Average power loss}}, \tag{1}$$

where f_o is the center frequency of a resonance characterized by a peak in the frequency response of the resonator (Matthaei et al., 1980). In practice the quality factor ($Q^m_{resonance}$) is measured by taking the center frequency and dividing it by its half-power bandwidth

$$Q^m_{resonance} = \frac{f_o}{\text{Bandwidth}}. \tag{2}$$

(Note that Eq. (2) only holds true where $Q^m_{resonance} \gg 1$.)

The quality factor of a resonator loaded with a test gas can be expressed as

$$\frac{1}{Q^m_{loaded}} = \frac{1}{Q_{gas}} + \frac{1}{Q_{vacuum}} + \frac{1}{Q_{probe1}} + \frac{1}{Q_{probe2}}. \tag{3}$$

Q_{gas} is the quality factor of the gas, which is related to the loss tangent and absorptivity of the gas by the relation

$$Q_{gas} = \frac{\epsilon'}{\epsilon''} = \frac{1}{\alpha}\frac{\pi}{\lambda}, \tag{4}$$

where ϵ' and ϵ'' are the real and imaginary parts of the permittivity of the gas mixture, α is the absorptivity (Nepers/km) and λ is the wavelength (km) (see, e.g. Pozar, 1998). Q_{vacuum} is the quality factor of the just the cavity under vacuum, and Q_{probe1} and Q_{probe2} represent the effects of coupling losses from the two probes on the quality factor of the resonator (Matthaei et al., 1980). Given that the resonator is symmetric, and the coupling probes are the same size and dimensions, it is assumed that $Q_{probe1} = Q_{probe2}$. This value is now referred to as $Q_{coupling}$ and is determined by measuring the transmission losses in the system, or transmissivity of the system $t = 10^{-S/10}$ where S is the insertion loss of the resonator in decibels (dB) at the frequency of a resonance. Using the following relations, the value of $Q_{coupling}$ is found via

$$t = \left(2\frac{Q^m}{Q_{coupling}}\right)^2, \tag{5}$$

$$\frac{1}{Q_{coupling}} = \frac{\sqrt{t}}{2Q^m}, \tag{6}$$

where Q^m is a measured quality factor (Matthaei et al., 1980). The value for Q_{vacuum} is related to the measured quality factor under vacuum (Q^m_{vacuum}) conditions by

$$\frac{1}{Q^m_{vacuum}} = \frac{1}{Q_{vacuum}} + \frac{1}{Q_{probe1}} + \frac{1}{Q_{probe2}}. \tag{7}$$

After substitution of Eq. (6) into Eqs. (3) and (7), the value of Q_{gas} is given by

$$\frac{1}{Q_{gas}} = \frac{1-\sqrt{t_{loaded}}}{Q^m_{loaded}} - \frac{1-\sqrt{t_{vacuum}}}{Q^m_{vacuum}}, \tag{8}$$

where t_{loaded} and t_{vacuum} are the transmissivity values of the loaded and vacuum measurements. One could directly calculate Q_{gas} assuming that the center frequency of a resonance does not change with the addition of a test gas. It is known, however, that this is not the case. An effect known as dielectric loading which is related to the refractive index of a gas present will change the center frequency of the resonance. This effect can be compensated by using a tunable resonator (e.g., Ho et al., 1966; Morris and Parsons, 1970); However, in doing this the coupling properties of the resonator can change, resulting in a error prone measurement of Q_{gas}. In place of a measurement of Q under vacuum conditions (Q^m_{vacuum}), one can measure the Q in the presence of a microwave transparent gas with the same refractive index as the test gas. The amount of microwave transparent gas added can be used to tune the center frequency of the resonator. This allows for a "frequency matched" value replacing the "vacuum" terms in Eq. (8) with "matched" terms. After making the appropriate substitution from Nepers/km to dB/km (1 Neper/km = 2 optical depths $km^{-1} = 2 \times 10\log_{10}(e) \approx 8.686$ dB/km) yields the expression used for calculating absorption

$$\alpha = 8.686\frac{\pi}{\lambda}\left(\frac{1-\sqrt{t_{loaded}}}{Q^m_{loaded}} - \frac{1-\sqrt{t_{matched}}}{Q^m_{matched}}\right)(\text{dB/km}), \tag{9}$$

where the wavelength λ has units of km (DeBoer and Steffes, 1996).

The dielectric loading of a resonance also gives information regarding the refractive index of a gas. For most gases the index of refraction (n) is usually close to unity. As a result the refractivity of a gas is given by multiplying the residual $n-1$ by 10^6, or

$$N = 10^6(n-1), \tag{10}$$

where N is the refractivity of a gas. The measurement of refractivity uses the dielectric loading principle discussed previously, and is calculated by a more direct method than absorption. The refractivity is measured using

$$N = 10^6\frac{f_{vacuum} - f_{gas}}{f_{gas}}, \tag{11}$$

where f_{vacuum} is the center frequency of a resonance measured under vacuum, and f_{gas} is the center frequency measured with a test gas (Tyler and Howard, 1969). Eq. (11) is only valid for values of refractive index (n) close to unity.

The center frequencies of a Transverse Electric (*TE*) or Transverse Magnetic (*TM*) mode resonance in a cylindrical cavity resonator are calculated using

Please cite this article in press as: Karpowicz, B.M., Steffes, P.G. In search of water vapor on Jupiter: Laboratory measurements of the microwave properties of water vapor under simulated jovian conditions. Icarus (2011), doi:10.1016/j.icarus.2010.11.035

$$f_{TE(N,M,L)} = \frac{c}{2\pi\sqrt{\mu_r \epsilon_r}} \sqrt{\left(\frac{p_{n,m}}{r}\right)^2 + \left(\frac{\pi L}{h}\right)^2}, \quad (12)$$

$$f_{TM(N,M,L)} = \frac{c}{2\pi\sqrt{\mu_r \epsilon_r}} \sqrt{\left(\frac{q_{n,m}}{r}\right)^2 + \left(\frac{\pi L}{h}\right)^2}, \quad (13)$$

where c is the speed of light (cm/s), μ_r and ϵ_r are the real parts of the relative permeability and permittivity of the medium contained inside the resonator, r and h are the interior radius and height of the resonator (cm), $q_{n,m}$ is the mth zero of the nth order bessel function, and $p_{n,m}$ is the first derivative of the mth zero, nth order bessel function of the first kind (Pozar, 1998). In this work only *TE* modes are measured due to their high quality factors. In fact most *TM* modes have been intentionally suppressed to further reduce interference with the neighboring *TE* modes (Hanley, 2008). The resonant frequencies reflect the changes in resonator physical dimensions due to thermal expansion or physical compression.

3. Measurement system

The Ultra-High Pressure System is shown in schematic form in Fig. 1. The system is composed of a pressure vessel (which contains the microwave resonator) custom built by Hays Fabrication and Welding (Springfield, Ohio), a water reservoir made of a T-304 stainless steel pipe 46 cm long and 3.8 cm in diameter, a Grieve® industrial oven model AB-650 (maximum temperature 343 °C), two Matheson® regulators (Model 3030-580 for Ar/He, and 3030-350 for H_2), two Omega® DPG7000 pressure gauges (one rated from 0 to 2 bars absolute, the other rated to 20 bar), an Omega® PX1009L0-1.5KAV pressure transducer capable of measuring up to 103 bars at 315 °C, and an Omega® thermocouple probe (TC-T-NPT-G-72). Valves rated for high temperature and pressure were used throughout the system.

The custom pressure vessel was designed with two 1.27 cm ($\frac{1}{2}$ in.) NPT input ports for gas delivery, one 6.35 mm ($\frac{1}{4}$ in.) NPT port for the thermocouple, and two CF-1.33 flanges measuring 3.38 cm (1.33 in.) in diameter for microwave feedthroughs. The pressure vessel was hydro-tested by Hays Fabrication and Welding with all input flanges, and feedthroughs at a pressure of 100 bars. In place of a standard rubber or viton O-ring a composite (glass fiber/NBR) KLINGERsil® C-4430 is used to seal the pressure vessel along with 20 nuts 6 cm (2-3/8 in.) in diameter torqued to 1762 N-m (1300 lb-ft) of torque. The vessel is constructed out of a 30.48 cm section of schedule 100 pipe which is 35.56 cm (14 in.) in diameter (outer dimension). On one end an elliptical head is welded to the bottom giving the vessel a maximum interior height of 46.04 cm (18-$\frac{1}{8}$ in.). The top is a ANSI class 900 flange 10.16 cm (4 in.) thick, with a top plate which is 9.2 cm (3-$\frac{5}{8}$ in.) thick. The vessel has a volume of 32.3 l, and weighs approximately 544.3 kg.

The weight of the pressure vessel (544.3 kg) and the shipping weight of the oven (739 kg) far exceeded the load capacity of our laboratory floor. After careful analysis it was determined that an outdoor concrete pad on which a decommissioned crane once stood, would be the ideal location for such a load. Thus, all system components except for the microwave network analyzer, sensor monitors, and the control computer are placed outdoors, protected by a metallic shed.

Over the course of the measurement campaign, some additions were made to the system described above. First, the 6.35 mm ($\frac{1}{4}$ in.) thermocouple probe (TC-T-NPT-G-72) was replaced by a high temperature thermometer/hygrometer (JLC international® EE33-MFTI-9205-HA07-D05-AB6-T52) for experiments 5–8 and experiments 14–17, so as to provide an independent, secondary measure of water vapor density. The high temperature thermometer/hygrometer was inserted into the 12.7 mm ($\frac{1}{2}$ in.) exhaust port of the pressure vessel. In place of the $\frac{1}{4}$ in. thermocouple probe, a $\frac{1}{4}$ in. line was used as a replacement exhaust port (shown as a dotted line in Fig. 1). The limited temperature range of the hygrometer/temperature sensor required that a another sensor be used above 475 K. The hygrometer/temperature sensor was replaced by a high precision Omega® Resistance Temperature Detector (RTD) (PR-11-2-100-1/8-9-E).

3.1. The data acquisition system

While developing the data acquisition and microwave systems for the atmospheric simulator, two major factors were considered: pressure, and temperature ratings. A schematic of the cables, and measurement devices used is shown in Fig. 2. The microwave

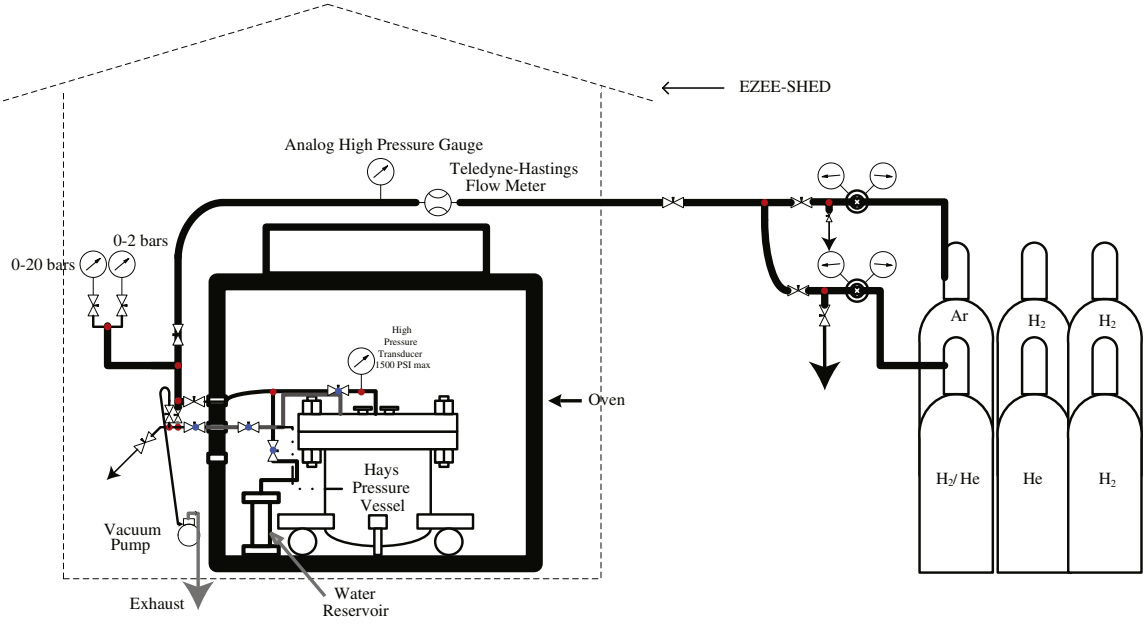

Fig. 1. The Georgia Tech Ultra-High Pressure System.

Please cite this article in press as: Karpowicz, B.M., Steffes, P.G. In search of water vapor on Jupiter: Laboratory measurements of the microwave properties of water vapor under simulated jovian conditions. Icarus (2011), doi:10.1016/j.icarus.2010.11.035

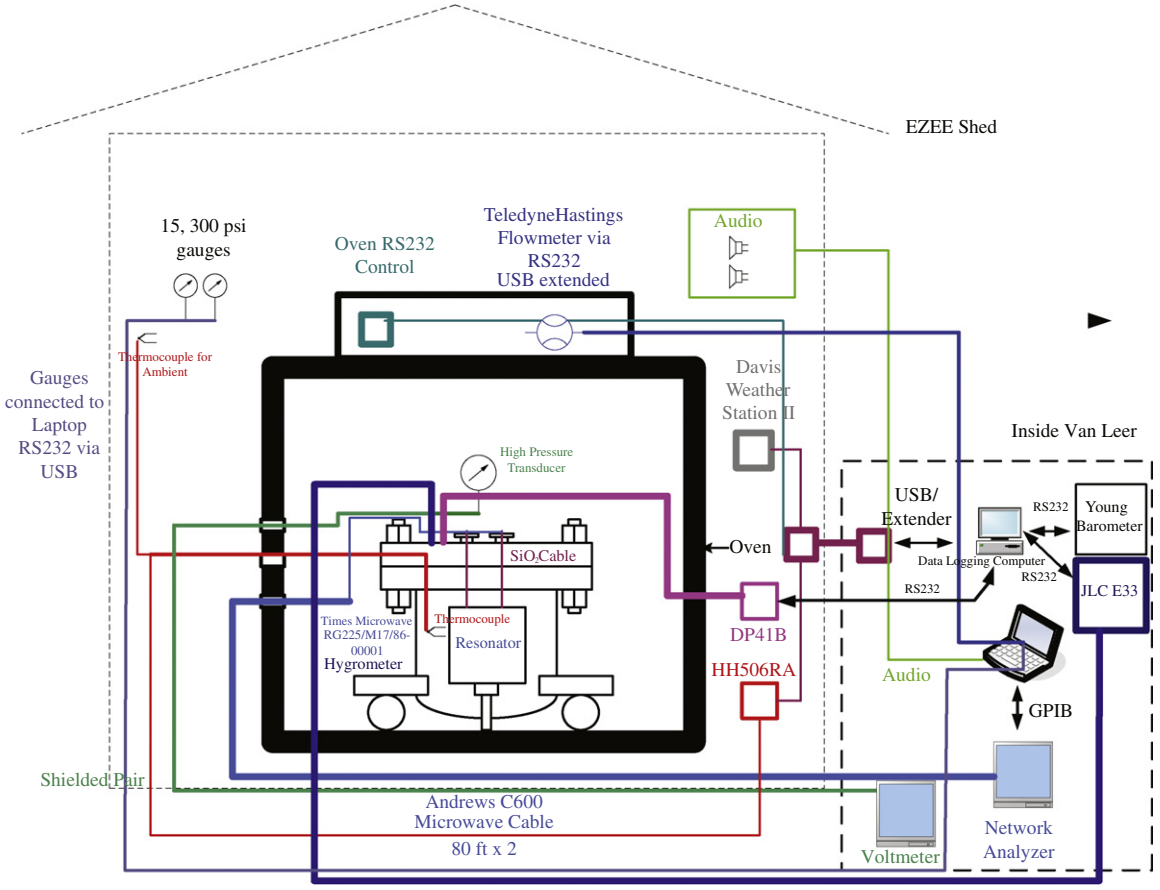

Fig. 2. The microwave and data acquisition system.

resonator shown in Fig. 2 has been used in several studies, most recently it has been used in studies by Hanley (2008) and Hanley and Steffes (2007). The resonator is a cylindrical cavity resonator with an interior height of 25.75 cm, and an interior radius of 13.12 cm. The resonator is connected to Ceramtec® feedthroughs within the pressure vessel, by SiO_2 microwave cables (Times Microwave®). They were selected to withstand the highest temperatures possible, 600 °C. On the exterior of the pressure vessel two SMA Ceramtec feedthroughs (16545-01-CF) both rated to 103 bars and 350 °C are used. Both Ceramtec® feedthroughs are backed by fully annealed copper gaskets. Two 1 m long sections of Times Microwave M17/86-00001 (formerly known as RG-225), then connect to type-N panel mounts on the outside of the oven. Two sections of Andrews® CNT 600 microwave cable (of 24 m in length) are connected to the type N bulkheads on the oven back to the Agilent® E5071C network analyzer. The CNT 600 cable is not exposed to an extreme environment, thus its maximum operating temperature of 85 °C is sufficient for our application. Use of the long microwave cable extension is required to ensure temperature stability of the Agilent® E5071C network analyzer by placing it within the laboratory environment. The *S* parameters measured by the network analyzer are read in via GPIB to the data acquisition computer.

In addition to the microwave measurement system, there are the pressure and temperature measurement systems. Both systems make use of an extended USB bus which allows the data acquisition computer to remain inside the laboratory. The temperature measurement system is composed of an Omega® HH506RA temperature reader connected to two type T thermocouples (one connected inside the pressure vessel and one on the pipes for ambient temperature). The temperature reader is connected to an RS-232/USB converter which is then connected to the USB bus within the EZEE shed. The Omega® DPG7000 pressure gauges are read via two USB webcams connected to the USB bus. Finally the voltage from the high pressure transducer is read in via a shielded twisted pair back into the laboratory where the voltage is read in by an HP 34401A multimeter. The data acquisition computer reads in the voltage from the multimeter via GPIB. For calibration purposes in the initial setup, a Davis® Weather Station II, with a barometer placed within the EZEE® shed, and connected to the USB bus via an RS232/USB converter was used to measure barometric pressure to a precision of ±1.7 mbar. However, a strong storm on August 1, 2008 resulted in some damage to the EZEE® shed, along with the functionality of the Davis® Weather Station II. A Young® 61202L barometric pressure sensor was purchased to replace the Davis® Weather Station II. To prevent further damage, and keep the sensor operating under conditions which maximize its precision (±0.3 mbar at 20 °C), the sensor is placed inside the laboratory and connected to a computer via RS232.

As time went on, our knowledge of available sensors accumulated. We discovered that an affordable line of pressure gauges which measured absolute pressure (rather than pressure relative to ambient), with the same precision as the Omega® DPG7000 series were available. The GE Sensing®/Druck® DPI-104 gauge has a 0.05% of full scale precision (≈0.001 bar for the 2 bar gauge, and ≈0.010 bar for the 20 bar gauge), has the option to be powered externally, and has an RS-232 interface for data acquisition. The DPG7000 series gauges required correction for local atmospheric pressure, replacing AAA batteries on a regular basis, and only display pressure (the only data acquisition interface is the experimenter). While the improvements over the DPG7000 series gauges may appear to be mostly a matter of convenience, the switch from relative to absolute pressure eliminates any

Please cite this article in press as: Karpowicz, B.M., Steffes, P.G. In search of water vapor on Jupiter: Laboratory measurements of the microwave properties of water vapor under simulated jovian conditions. Icarus (2011), doi:10.1016/j.icarus.2010.11.035

Table 1
Instruments used and associated precision.

Instrument	Range (°C)	Measurement parameter	Precision (3σ)
Omega® DPG7000[a]	−18 to 65	Pressure 0–2 bars (Vacuum – 15 psig)	±0.05% FS
Omega® DPG7000[a]	−18 to 65	Pressure 1–20 bars (Ambient – 300 psig)	±0.05% FS
Omega® PX1009L0-1.5KAV	−18.3 to 343.3	Pressure 0–103 bars (0–1500 psia)	±0.06% FS
Omega® HH506RA	−20 to 60	Temperature −200 to 400 °C	±(0.05% rdg + 0.3 °C)
Omega® PR-11-2-100-1/8-9-E	−50 to 450	Temperature −50 to 450 °C	±(0.15 + 0.002 rdg) °C
Omega® DP41B	0–50	Temperature −200 to 900 °C	±0.2 °C
Type T Thermocouple	−200 to 400	Temperature −200 to 400 °C	Greater of ±1.0 °C or 0.75% rdg
Agilent® E5071C	~20	*S* parameters	See Discussion
HP® 34401A multimeter	~20	Voltage (output from transducer)	±(0.0050% rdg + 0.0035% range)
Davis® Weather Station II[b]	−20 to 60	Barometric pressure, mbars	±1.7 mbar @ 20 °C
Young® 61202L	~20	Barometric pressure, mbars	±0.3 mbar @ 20 °C
JLC® EE33-MFTI	−40 to 180	Humidity (RH%)	±(1.5% + 0.015∗RH)
JLC® EE33-MFTI	−40 to 180	Temperature (°C)	±0.3–0.5 °C
GE sensing®/Druck® DPI-104	−10 to 50	Pressure 0–2 bars (0–30 psia)	±0.05% FS
GE sensing®/Druck® DPI-104	−10 to 50	Pressure 0–20 bars (0–300 psia)	±0.05% FS
Teledyne-Hastings® HFM-I-401	−20 to 70	Flowrate 0–10 slm, operates up to 1500psi	±(0.2% FS + 0.5% rdg)

[a] Replaced in favor of DPI-104.
[b] Replaced with Young® 61202L.

uncertainty or error when correcting the relative measurements to obtain absolute pressure. Table 1 shows all instrumentation used for the experiments along with their operating conditions, and precision. Every parameter measured has an associated precision (see Table 1) which is included in the online data set.

4. Measurement process

The measurement process involved an extensive series of measurements under deep jovian conditions with temperatures in the range 333–525 K, and pressures up to 100 bars. A possible dry jovian adiabatic temperature–pressure overlayed with pressure–temperature measurement points are shown in Fig. 3. As shown in Fig. 3, there is an extensive number of measurement points (each involving hundreds of data points) covering a wide range of temperature and pressure.

The measurement process is quite involved and time consuming. While extensive lengths have been taken to automate processes, the experimenter still must be actively involved in each stage in the process. The first step in the process involves drawing a vacuum in the system, which took 8–24 h depending upon what constituents were in the high pressure system prior to drawing a vacuum. While the vacuum pump is drawing a vacuum, the experimenter must periodically monitor the temperature within the pressure vessel, and make slight adjustments to the temperature to ensure the temperature is constant just prior to taking a vacuum measurement of the microwave resonator response. While there is a computer control of temperature, there are a number of factors which contribute to a fluctuation in temperature within the pressure vessel. First, the thermocouple for the temperature controller is in the air stream of the oven, not inside the pressure vessel. This allows the oven to control the temperature within a short period of time, but is not necessarily the temperature within the pressure vessel. Second, the high pressure system and oven are outdoors (covered by a steel EZEE shed), and are subject to large ambient temperature swings which result in a temperature offset. This offset in temperature is a combined effect of the temperature controller response and of radiation of heat from pipes and small orifices

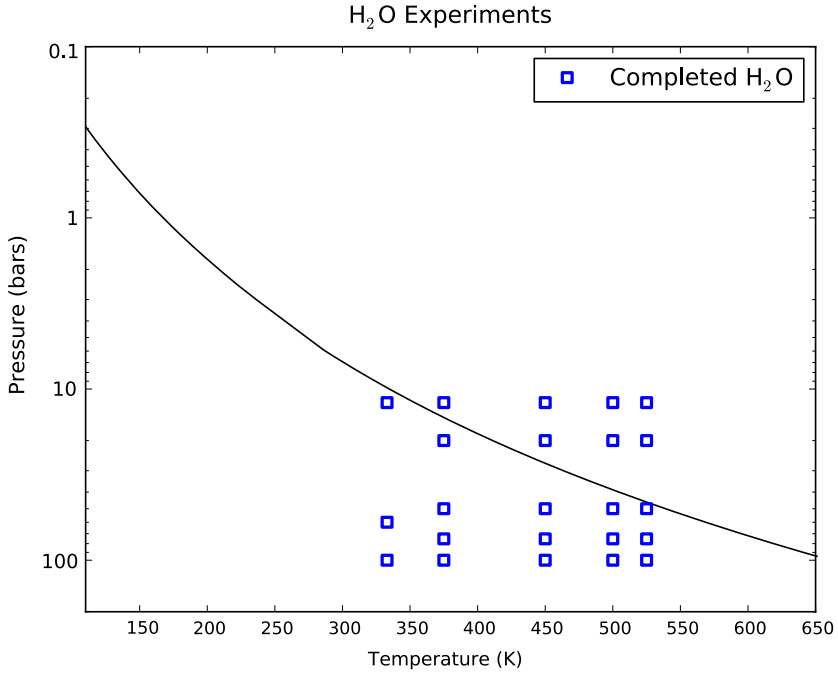

Fig. 3. Dry jovian adiabatic temperature–pressure profile along with *T–P* space of microwave opacity measurements.

Please cite this article in press as: Karpowicz, B.M., Steffes, P.G. In search of water vapor on Jupiter: Laboratory measurements of the microwave properties of water vapor under simulated jovian conditions. Icarus (2011), doi:10.1016/j.icarus.2010.11.035

in the oven (for cable feedthroughs etc). The observed trend is that for an increase in ambient temperature of a few °C, the oven will decrease in temperature between 0.2 °C and 0.5 °C, with the opposite being true for a decrease in ambient temperature. Once the experimenter has determined that the temperature is stable, a measurement is taken of the spectral response of the microwave resonator. The quality factor from the vacuum measurement is used to compute an error budget as described in Section 5.

Once a measurement of the microwave resonator's spectral response has been taken, the experimenter quickly opens the oven, closes off valves which admit/vent gas to the pressure vessel (inside the oven), and opens the valve to the water reservoir shown in Fig. 1. The water reservoir was filled with distilled water, ACS Reagent Grade with ASTM D 1193 specifications for reagent water, type II (manufactured by Ricca Chemical Company). The experimenter closely monitors either the pressure reading from the transducer or the hygrometer, and closes the valve to the water reservoir once the desired water vapor pressure (always below the saturation vapor pressure) is reached. The experimenter quickly closes the door to the oven and monitors both the hygrometer reading (when available), temperature and the center frequency of a few key resonances. Stabilization of the hygrometer reading and the center frequencies of the resonances (approximately 6–8 h) indicates that the water vapor is well mixed within the pressure vessel, and a second measurement of the spectral response of the resonator is taken. This spectral response is used to compute Q^m_{loaded} in Eq. (9) over several resonances in the resonator, and is used to compute the microwave opacity of pure water vapor at the center frequencies of those resonances.

After completing the measurement of pure water vapor, the experimenter conducts what is referred to as a "buffer measurement" of the water vapor pressure. While there is a measurement of water vapor pressure made by the transducer, and hygrometer (when available), this measurement is not as precise as one can make with either the DPG-7000, or the DPI-104 vacuum/pressure gauges. The "buffer measurement" technique provides an independent measurement of water vapor pressure by loading the small section of pipe connecting to the pressure gauges with a gas at a pressure slightly greater than the pressure indicated by either the transducer, or hygrometer. The experimenter then quickly opens the door to the oven, opens the valve to the pressure vessel, and records the pressure from the pure water vapor (plus a minute correction for the neutral gas in the buffering) indicated by the DPG-7000 or DPI-104 gauges, and then closes the valve. Since the pressure in the connecting pipe exceeds the water vapor pressure, no water vapor escapes into the pressure gauge, which is at ambient temperature (Fahd, 1992). The experimenter then adds Hydrogen and Helium to the pressure vessel until the next desired pressure is reached. Once the desired pressure is reached the experimenter shuts the valve inside the oven, and closes the door to the oven. The experimenter then waits another 6–8 h for the system to stabilize before taking another measurement of the resonators spectral response. The process described is repeated with a direct measurement of pressure using the transducer once the pressure limit of either the DPI-104, or DPG-7000 (approximately 20 bars) is exceeded.

Once the maximum pressure in an experiment has been reached, the experimenter reverses the process by venting the gas mixture, giving a second group of measurements. By assuming no preferential venting of any constituent, the reduced pressure mixtures would have a constant mixing ratio of water vapor, and hydrogen/helium. As with previous experiments (involving ammonia, Hanley et al., 2009), when the gas mixture is vented the partial pressure of water vapor drops. Unfortunately, this leads to desorption of water vapor which had previously adsorbed to the metallic surfaces, elevating the water vapor mixing ratio. As a result the measurements conducted during the venting cycle have large uncertainties, and are not used in the model development. Once the remaining gas is vented, a vacuum is drawn in the system. A second measurement of the system's spectral response is taken after 24 h under vacuum conditions.

The next step in the process is to add a microwave transparent gas so as to dielectrically match the center frequencies of the measured resonances. In all of the experiments, argon was used due to its high refractivity, reducing the amount of gas necessary to match each pressure. The process involves reading the previous measurement of the center frequency of each resonance taken with the test gas present, and then adding argon until the center frequency of the resonator is matched. The experimenter must wait a few hours when adding large amounts of argon so that the system will thermally stabilize. Subsequently, the experimenter carefully adds or removes gas to precisely match the center frequency measured when the test gas mixture was present. This process is aided by a series of tones produced by the data acquisition computer to help the experimenter reach the center frequency. The measured spectral response of each resonance is used to compute $Q^m_{matched}$ and $t_{matched}$ in Eq. (9). Once all resonances have been matched over all pressure conditions, the system is again vacuumed, and measurements of the resonator properties are again taken.

The final step in the measurement process is to correct the measurements of transmissivity for losses in the cables. This requires that the experimenter open the oven, disconnect the microwave cables from the resonator and connect a female-to-female sma adapter (thru load) in place of the resonator. The experimenter then closes the oven door, and waits until the temperature stabilizes within the oven. Once the oven reaches the desired temperature the cables losses are measured and used to correct t_{loaded}, and $t_{matched}$ in Eq. (9). The entire process, from drawing the initial vacuum to the final transmissivity measurement, takes about 1 week.

5. Uncertainties

There are five uncertainties for measuring the absorptivity: instrumentation errors and electrical noise (Err_{inst}), errors in dielectric matching (Err_{diel}), errors in transmissivity measurement (Err_{trans}), errors due to resonance asymmetry (Err_{asym}), and errors in the measurement conditions resulting from uncertainty in temperature, pressure, mixing ratio, and compressibility (Err_{cond}). The work of Hanley and Steffes (2007) and Hanley (2008) thoroughly describe the computation of errors, however, a brief overview of how these errors are computed in the current work is of some interest.

The instrumentation errors considered in Err_{inst} are limited to instrumentation errors associated with the microwave test equipment. Over time frequency sources (like clocks) exhibit drift over time, which introduce errors into the measurement of frequency. Two parameters of interest in calculating Err_{inst} are the error in measuring the center frequency of a resonance (Err_o) and the error in measuring the bandwidth of a resonance (Err_Δ). The instrument used in these experiments is the same Agilent E5071C-ENA Vector Network Analyzer used in Hanley (2008). The value for Err_o (3σ error) is calculated following Hanley (2008)

$$Err_o = f_{measured}\left(5\times10^{-8}+5\times10^{-7}\times \textit{years since calibrated}\right)(\text{Hz}), \quad (14)$$

with the measured frequency given in Hz. Agilent does not provide an error calculation for its E5071C-ENA Vector Network Analyzer, therefore the approach of Hanley (2008) is followed using

Please cite this article in press as: Karpowicz, B.M., Steffes, P.G. In search of water vapor on Jupiter: Laboratory measurements of the microwave properties of water vapor under simulated jovian conditions. Icarus (2011), doi:10.1016/j.icarus.2010.11.035

$$Err_\Delta = \sqrt{2}BW_{measured}\left(5\times10^{-8}+5\times10^{-7}\times years\ since\ calibrated\right)(\mathrm{Hz}), \quad (15)$$

with the measured bandwidth given in Hz, and Err_Δ is a 3σ error.

One final source of error that must be accounted for before calculating Err_{inst} is the uncertainty in the mean of the measurement population Err_n. For each resonance 30 sweeps are taken, the standard deviations of the bandwidths measured for the 30 sweeps are computed, and Err_n is computed for each resonance as

$$Err_n = \frac{2.045}{\sqrt{30}}s_n, \quad (16)$$

where s_n is the standard deviation of the Bandwidth measurement of a resonance over 30 sweeps, and 2.045 is the 95% confidence coefficient for 30 samples. For further details on computing Err_n see Hanley (2008).

The worst case error for instrumentation is given by

$$Err_{inst} = \pm\frac{8.686\pi}{\lambda}Err_\psi\ (\mathrm{dB/km}) \quad (17)$$

with λ is the wavelength (km), and Err_ψ is calculated as

$$Err_\psi = \sqrt{\Gamma_l^2+\Gamma_m^2-2(\Gamma_l\Gamma_m)}. \quad (18)$$

The remaining terms in Eq. (18) are calculated using

$$\Gamma_i^2 = \frac{\gamma_i^2}{f_{o,i}^2}\left[\frac{Err_o^2}{Q_i^2}+Err_\Delta^2+Err_{N_i}^2+\frac{2Err_oErr_\Delta}{Q_i}\right], i=l,m, \quad (19)$$

$$\Gamma_l\Gamma_m = -\frac{\gamma_l\gamma_m}{f_{o,l}f_{o,m}}\left[\frac{Err_o^2}{Q_lQ_m}+Err_\Delta^2+\frac{Err_oErr_\Delta}{Q_l}+\frac{Err_oErr_\Delta}{Q_m}\right], \quad (20)$$

$$Q_i = \frac{f_{o,i}}{BW_i}, i=l,m \quad (21)$$

where subscripts l and m represent loaded and matched cases, and γ, f_o, and BW represent the $1-\sqrt{t}$ terms from Eq. (9), the resonance center frequency, and resonance bandwidth, respectively. Values for Err_o and Err_Δ are scaled by factor of $\frac{2}{3}$ to yield 2σ uncertainties.

Errors in dielectric matching (Err_{diel}) result from imprecise alignment of the center frequency of the matched measurement with that of the loaded measurement. Even though the gas used for matching is lossless, the quality factor measured can vary slightly. The magnitude of this effect is calculated by comparing the quality factors for three vacuum measurements to the matched quality factor

$$\left(\frac{dQ}{df}\right)_i = \left|\frac{Q_{vacuum,i}-Q_{matched}}{f_{vacuum,i}-f_{matched}}\right|, \text{for } i=1,2, \text{ and } 3. \quad (22)$$

The maximum of the three values is then used to calculate a dQ value

$$dQ = \left(\frac{dQ}{df}\right)_{max}|f_{loaded}-f_{matched}|, \quad (23)$$

where f_{loaded} and $f_{matched}$ are the center frequencies of the resonance under loaded and matched conditions, respectively. The error in dielectric matching is then computed by propagating $\pm dQ$ through Eq. (9)

$$Err_{diel} = \left|8.686\frac{\pi}{\lambda}\left[\left(\frac{1-\sqrt{t_{loaded}}}{Q^m_{loaded}}-\frac{1-\sqrt{t_{matched}}}{Q^m_{matched}+dQ}\right)-\left(\frac{1-\sqrt{t_{loaded}}}{Q^m_{loaded}}-\frac{1-\sqrt{t_{matched}}}{Q^m_{matched}-dQ}\right)\right]\right|. \quad (24)$$

Most commonly, the largest uncertainty in these measurements comes from the process of disconnecting and reconnecting cables during the transmissivity measurements. The error is found by taking the appropriate statistics about the measured transmissivity. The cables to the pressure vessel feedthroughs are disconnected from the resonator and then connected in a thru configuration so that the cable losses are measured for each resonance. The cables are disconnected and reconnected, the cables losses are measured again, and the process is repeated a third time to generate three samples. The error in measured transmissivity is given by

$$Err_{mt} = \frac{4.303}{\sqrt{3}}s_n, \quad (25)$$

where s_n is the standard deviation of the cable loss measurements (in dB), and 4.303 is the 95% confidence coefficient for three samples. While Err_{mt} takes into account the variation in the cables which can be connected and reconnected, it does not account for the variabilities in the cables within the pressure vessel which can't be removed. To account for the additional uncertainty from temperature variation in those cables, a value of 0.25 dB is assumed based on worst-case models of cable performance. An additional 0.5 dB uncertainty related to variations in the cable losses due to temperature variations in the 15 m long outdoor section of each 24 m cable is also added. The resulting value for the total uncertainty in insertion loss is

$$Err_{insertion\ loss} = \sqrt{Err_{mt}^2+0.25^2+0.5^2}. \quad (26)$$

The error in insertion loss is used to find the error in transmissivity

$$Err_{t,i} = \frac{1}{2}\left(10^{-(S_i-Err_{insertionloss})}-10^{-(S_i+Err_{insertion\ loss})}\right), \quad i=l,m \quad (27)$$

where subscript i represents the loaded and matched cases and S is the insertion loss of the resonator. This is used to map the 2σ uncertainty in opacity which gives

$$Err_{trans} = \frac{8.686}{2}\times\frac{\pi}{\lambda}\left(\frac{\sqrt{t_l+Err_{t,l}}-\sqrt{t_l-Err_{t,l}}}{Q^m_{loaded}}-\frac{\sqrt{t_m-Err_{t,m}}-\sqrt{t_l+Err_{t,m}}}{Q^m_{matched}}\right) \quad (28)$$

The final source of uncertainty is that which arises from the asymmetry of a resonance. This is accounted for by first calculating the bandwidth based upon higher and lower halves of the resonance

$$BW_h = 2(f_h-f_c) \quad (29)$$

$$BW_l = 2(f_c-f_l) \quad (30)$$

where BW_h and BW_l are the equivalent full bandwidths based on assuming symmetry of the high and low sides of the resonance, f_h is the frequency at the half power point on the upper portion of the resonance, f_l is the frequency at the half power point on the lower portion of the resonance, and f_c is the center frequency. The difference between opacities calculated using BW_h and BW_l are treated as a 2σ error defined as Err_{asym} and is expressed as

$$Err_{asym} = \left|8.686\frac{\pi}{\lambda}\left[\left(\frac{1-\sqrt{t_{loaded}}}{Q^m_{loaded}(BW_h)}-\frac{1-\sqrt{t_{matched}}}{Q^m_{matched}(BW_h)}\right)-\left(\frac{1-\sqrt{t_{loaded}}}{Q^m_{loaded}(BW_l)}-\frac{1-\sqrt{t_{matched}}}{Q^m_{matched}(BW_l)}\right)\right]\right|, \quad (31)$$

where $Q^m_{loaded}(BW_h)$ and $Q^m_{loaded}(BW_l)$ are the loaded quality factors evaluated using the bandwidth computed using the higher and lower half of the resonance, respectively. The values $Q^m_{matched}(BW_h)$, and $Q^m_{matched}(BW_l)$ are the matched quality factors computed using the higher and lower half of the resonance, respectively.

The uncertainties in measurement conditions Err_{cond} do not directly affect the measurements of the microwave opacity, and thus are not included in the data set of measured absorptivities described in Section 7. However, they can affect the ability to fit a

Please cite this article in press as: Karpowicz, B.M., Steffes, P.G. In search of water vapor on Jupiter: Laboratory measurements of the microwave properties of water vapor under simulated jovian conditions. Icarus (2011), doi:10.1016/j.icarus.2010.11.035

model which includes the effects of pressure, temperature, concentration and compressibility on the absorbing properties of the test gas mixture, which are discussed in Section 9. The value of Err_{cond} is found using

$$Err_{cond} = \sqrt{Err_{Temp}^2 + Err_P^2 + Err_C^2}, \quad (32)$$

with Err_{Temp}, Err_P, and Err_C representing the effects on opacity of the 2σ uncertainties in temperature, pressure and water vapor abundance, respectively. Each of those is calculated by taking the maximum modeled opacity with each uncertainty minus the minimum modeled opacity and halving the difference. Err_{cond} is not used in our error budget for the measurement, and is used only as a point of reference for a given opacity model.

Thus, the 95% confidence measurement uncertainty is for the absorptivity measurements calculated as per (Hanley et al., 2009).

$$Err_\alpha = \sqrt{Err_{inst}^2 + Err_{diel}^2 + Err_{trans}^2 + Err_{asym}^2}. \quad (33)$$

While the theoretical computation of refractivity using an ideal resonator as given in Eq. (11) is relatively simple, the actual calculation, and propagating errors using a resonator that can deform with temperature and pressure is slightly more complex. The extensive set of measurements conducted allows us to model the temperature dependence of the cavity resonator under vacuum conditions. Hanley (2008) showed that the height (h) and radius (r) of the cavity resonator can be represented as

$$r_T = a_o + a_1 T + a_2 T^2 \ (\text{cm}), \quad (34)$$

$$h_T = b_o + b_1 T \ (\text{cm}), \quad (35)$$

where a_i, and b_i are empirically derived coefficients. These coefficients are derived using all the conducted vacuum measurements and fitting Eq. (12) with the values of a_i, and b_i as free parameters. The derived parameters are given in Table 2. The overall correlation coefficient (R^2) is 0.999999916598402. The calculation of the effect of changing dimensions on the resonance frequencies is described by (Pozar, 1998). In a future paper, results for water vapor refractivity will be presented.

6. Effects of gas compressibility

In previous works the Georgia Tech microwave measurement system constituents were always treated as ideal gases (e.g. Hanley et al., 2009; Mohammed and Steffes, 2003; Hoffman and Steffes, 2001; Joiner and Steffes, 1991). Unfortunately, the ideal gas law breaks down under high pressure, especially for gases such as H_2 and water vapor. To further add to this complexity mixtures have non-ideal interactions which vary as a function of their mole fraction, especially the components H_2 and water vapor (Seward et al., 2000; Rabinovich, 1995; Seward and Franck, 1981). This compromises the use of partial pressures alone to determine concentration. The volume occupied by the gas mixture under test in the pressure vessel must be determined to the highest precision possible such that the initial amount of water vapor added to the system can be determined.

A Teledyne-Hastings flowmeter with a flow "totalizer" function was purchased to monitor actual mass flow and aid in determination of the system volume. Three series of pVT measurements were conducted in this work: a series of measurements of Pure H_2 at a temperature of 375 K, a series of measurements of Pure H_2 at a temperature of 450 K, and a series of measurements with an H_2–H_2O mixture at 375 K, and 450 K. The maximum compressibility of the mixture used in our measurements was about 6.5% (indicating a compressibility factor of 1.065 vs. unity for an ideal gas), however, it was still necessary to include the effects of compressibility when developing a model for the microwave opacity from water vapor in a jovian atmosphere. Thus, the model developed describes opacity at a given frequency in terms of the temperature and the mass densities of each constituent, without reference to the actual pressure of the gas mixture.

The effects of compressibility have a more significant effect on the equation of state for jovian atmospheres, especially under the high pressures encountered in the deep atmosphere. A future paper will describe development of a new equation of state based on these measurements (see also Karpowicz, 2010). The experiments we conducted utilized a flowmeter with an accuracy of 0.2% of full scale plus an additional 0.5% of the flow reading. For our experiments, this corresponds to an accuracy of 1%.

Table 2
Empirically derived coefficients for Eqs. (34) and (35).

i	a_i	b_i
0	12.993000651099409	25.635264739431314
1	0.000498685501301	0.000412843042129
2	−0.000000332586042	–

7. Measurements conducted

The ultra-high pressure measurement data set for water vapor is the result of many hours repeating the process described in Section 5. The data set contains 17 measurement data sets. The measurement conditions for each experiment are summarized in Table 3. While conducting measurements three different mixtures of broadening gases were used. The first used water combined with a hydrogen/helium mixture premixed with a mole fraction of 13.5% helium (the jovian abundance as measured by von Zahn et al. (1998)). This mixture was used for experiments 1 and 2, and for a few pressures in experiments 7–9. The second type of mixture was for a pure mixture of Helium up to either 6 or 13 bars pressure, with remaining pressures using pure hydrogen. Finally, a measurement of water vapor in pure hydrogen was conducted to better decouple the interactions between hydrogen–water, and helium–water broadening.

As mentioned in Section 5, the data points taken while decreasing pressure were omitted owing to preferential venting of hydrogen/helium vs. water vapor, and are considered valid measurements of opacity, but are not used for fitting given we can't be certain of the water vapor mixing ratio. Also, experiment 17 is included in the data set only for reference, and is not used for fitting owing to the low opacity, scatter in the data set, and was the only experiment conducted at 333 K. The data set is available for download as an excel spreadsheet using the following url: http://users.ece.gatech.edu/psteffes/palpapers/karpowicz_data/water_data/h2o_data.xls. The data are organized with "tabs" and are split by experiment with data quality flags indicating, valid data (0), invalid data points (1), omitted data (preferential venting of H_2) (2).

8. Centimeter-wave opacity model

The new opacity model which is optimized using the highest quality data from our extensive measurement data set starts with a modification of the Rosenkranz (1998) model for water vapor. Rosenkranz (1998) was chosen as a starting point owing to the fact that it is frequently used for microwave remote sensing studies of Earth. The Rosenkranz model has a relatively simple form, and allowed us to modify continuum terms to fit our measurements. It may be possible to adapt models such as the MT_CKD (Payne et al., 2011) which have a stronger physical basis, however, the

Please cite this article in press as: Karpowicz, B.M., Steffes, P.G. In search of water vapor on Jupiter: Laboratory measurements of the microwave properties of water vapor under simulated jovian conditions. Icarus (2011), doi:10.1016/j.icarus.2010.11.035

Table 3
Summary of experiments conducted using the ultra-high pressure measurement system.

Experiment	Temperature (°K)	Max. pressure (bars)	Hydrogen–helium mixture	Water vapor pressure (bars)	Dates
1	376.1	21.2	Factory H_2–He Pre-mix 13.5% He	0.328	07/26/2008–08/09/2008
2	376.2	86.0	Factory H_2–He Pre-mix 13.5% He	0.322	08/13/2008–08/29/2008
3	376.3	96.1	846.5 g/m^3 He	0.396	09/2/2008– 09/11/2008
4	376.2	99.6	1691.4 g/m^3 He	0.384	9/30/2008–10/21/2008
5	376.2	96.6	1658.8 g/m^3 He	0.363	11/11/2008–11/26/2008
6	376.2	99.6	H_2 Only	0.444	11/28/2008–12/07/2008
7	451.2	101.1	Factory Pre-mix up to 20 bars	1.358	12/08/2008– 12/18/2008
8	451.2	99.3	Factory Pre-mix up to 20 bars	0.701	12/20/2008–1/23/2008
9	523.2	90.6	Factory Pre-mix up to 40 bars	3.290	1/26/2009– 2/16/2009
10	523.1	88.7	1077.9 g/m^3 He	1.856	2/18/2009–2/25/2009
11	498.2	87.8	H_2 Only	2.504	2/28/2009– 3/7/2009
12	498.2	87.4	1250.1 g/m^3 He	0.923	3/9/2009–3/14/2009
13	498.1	92.4	590.2 g/m^3 He	2.106	3/27/2009–4/2/2009
14	451.1	91.7	H_2 Only	1.149	4/8/2009– 4/18/2009
15	451.2	91.7	879.9 g/m^3 He	1.388	4/19/2009–4/25/2009
16	451.1	89.1	1386.8 g/m^3 He	0.744	4/26/2009–5/1/2009
17	333.0	82.1	1928.6 g/m^3 He	0.175	5/5/2009–5/10/2009

MT_CKD model is constrained by field measurements in wavelength bands ranging from the microwave to infrared in Earth's atmosphere. Additional information regarding the infrared/submillimeter absorption from water vapor in an H_2/He atmosphere would be required to develop a jovian version of the MT_CKD model. An updated version of the Rosenkranz (1998) model was provided by Dr. Philip Rosenkranz, and was heavily modified to fit our measurements. The model includes lines from the HITRAN database (Rothman et al., 2009) up to 916 GHz. The line centers, line intensities, line widths and temperature exponents are given in Table 4. Many line parameters have been updated since the original Rosenkranz (1998) paper and are provided in Table 4. Both the new jovian model presented in this work, and the Rosenkranz model share the same set of self broadening parameters. The contributions for line absorption is computed using

$$\alpha_{lines} = n_w \sum_{i=1}^{15} I_{o,i}\theta^{2.5}\exp(E_{o,i}(1-\theta))F_{VVW}(v_i, v, \Delta v_i)\ (\mathrm{km}^{-1}) \tag{36}$$

where n_w is the number density of water molecules in molecules per cubic centimeter weighted by the isotope fraction from O^{16} (0.997317), $I_{o,i}$ is the line intensity, $E_{o,i}$ is the temperature coefficient, θ is the standard $\frac{300}{T}$ where T is in degrees Kelvin, and F_{VVW} is the van Vleck-Weisskopf line shape given as

$$F_{VVW}(v_i, v, \Delta v_i) = \frac{1}{\pi}\frac{v}{v_i}\left[\frac{\Delta v_i}{(v_i - v)^2 + \Delta v_i^2} + \frac{\Delta v_i}{(v_i + v)^2 + \Delta v_i^2}\right]. \tag{37}$$

The value of Δv_i is computed using

$$\Delta v_i = P_{ideal,H_2O}\theta^{x_{H_2O,i}}\Delta v_{H_2O,i} + P_{ideal,H_2}\theta^{x_{H_2,i}}\Delta v_{H_2,i} + P_{ideal,He}\theta^{x_{He,i}}\Delta v_{He,i} \tag{38}$$

where $x_{H_2O,i}x_{H_2,i}$ and $x_{He,i}$ are the temperature exponents for water vapor, hydrogen, and helium, respectively. Likewise, the parameters $\Delta v_{H_2O,i}\Delta v_{H_2,i}$ and $\Delta v_{H_2O,i}$ are the line broadening parameters for water vapor, hydrogen, and helium, respectively. The line and broadening parameters are given in Tables 4 and 5. The values for $P_{ideal,H_2O}P_{ideal,H_2}$ and $P_{ideal,He}$ are the *ideal* pressures which are computed from the *density* of each constituent present. In the case of our experiments this is the density as computed by the equation of state developed in (Karpowicz, 2010). This will be the subject of a future publication, as the method used to derive the interaction parameters for H_2–H_2O requires a lengthy description. Once the density is computed the ideal pressure is computed as

$$P_{ideal,gas} = \frac{\rho_{gas}}{M_{gas}}R_{gas}T\ (\mathrm{bars}), \tag{39}$$

where ρ_{gas} is the density of the gas in grams per cubic meter, M_{gas} is the molecular weight of the gas (in grams per mole), R_{gas} is the ideal gas constant for the gas, and T is the Temperature in Kelvin. The value for R_{gas} is the generally accepted value of 8.314472×10^{-5} m^3 bar/K mol for H_2 (Leachman, 2007) and H_2O (Wagner and Pruß, 2002), however, the equation of state for helium requires the use of the older value 8.314310×10^{-5} m^3 bar/K mol (McCarty, 1990).

The broadening parameters for H_2 and He are taken from de Pater et al. (2005), and are given in Table 5.

Table 4
Self broadening line parameters for water vapor.

Line (GHz)	Line intensities ($I_{i,o}$)	Line widths ($\Delta v_{H_2O,i}$ in GHz/mbar)	Temperature exponent (x_{H_2O})	Temperature coefficient ($E_{o,i}$)
22.2351	0.1314×10^{-13}	0.01349	0.61	2.144
183.3101	0.2279×10^{-11}	0.01466	0.85	0.668
321.2256	0.8058×10^{-13}	0.01057	0.54	6.179
325.1529	0.2701×10^{-11}	0.01381	0.74	1.541
380.1974	0.2444×10^{-10}	0.01454	0.89	1.048
439.1508	0.2185×10^{-11}	0.009715	0.62	3.595
443.0183	0.4637×10^{-12}	0.00788	0.50	5.048
448.0011	0.2568×10^{-10}	0.01275	0.67	1.405
470.8890	0.8392×10^{-12}	0.00983	0.65	3.597
474.6891	0.3272×10^{-11}	0.01095	0.64	2.379
488.4911	0.6676×10^{-12}	0.01313	0.72	2.852
556.9360	0.1535×10^{-8}	0.01405	1.0	0.159
620.7008	0.1711×10^{-10}	0.011836	0.68	2.391
752.0332	0.1014×10^{-8}	0.01253	0.84	0.396
916.1712	0.4238×10^{-10}	0.01275	0.78	1.441

Please cite this article in press as: Karpowicz, B.M., Steffes, P.G. In search of water vapor on Jupiter: Laboratory measurements of the microwave properties of water vapor under simulated jovian conditions. Icarus (2011), doi:10.1016/j.icarus.2010.11.035

Table 5
Hydrogen and helium line broadening parameters for water vapor.

Line (GHz)	$\Delta\nu_{H_2}$ (GHz/bar)	$\Delta\nu_{He}$ (GHz/bar)	Temperature exponent (x_{H_2})	Temperature exponent (x_{He})
22.2351	2.395	0.67	0.900	0.515
183.3101	2.400	0.71	0.950	0.490
321.2256	2.395	0.67	0.900	0.515
325.1529	2.395	0.67	0.900	0.490
380.1974	2.390	0.63	0.850	0.540
439.1508	2.395	0.67	0.900	0.515
443.0183	2.395	0.67	0.900	0.515
448.0011	2.395	0.67	0.900	0.515
470.8890	2.395	0.67	0.900	0.515
474.6891	2.395	0.67	0.900	0.515
488.4911	2.395	0.67	0.900	0.515
556.9360	2.395	0.67	0.900	0.515
620.7008	2.395	0.67	0.900	0.515
752.0332	2.395	0.67	0.900	0.515
916.1712	2.395	0.67	0.900	0.515

While the line contributions are important, they are quite insignificant in the frequency range where our measurements were conducted. The feature which dominates in this frequency regime is the continuum absorption defined as:

$$\alpha_{continuum} = \alpha_{c,w} + \alpha_{c,f}, \tag{40}$$

where $\alpha_{c,w}$ is the continuum term from the water density, and $\alpha_{c,f}$ is the continuum term dependent upon the foreign gas present. The continuum term from water vapor is defined as

$$\alpha_{c,w} = C_w P^2_{ideal,H_2O}\theta^{x_{w,continuum}} f^2 + C'_w P^{n_{continuum}}_{ideal,H_2O}\theta^{x'_{continuum}} f^2 \ (\mathrm{km}^{-1}), \tag{41}$$

where C_w is an empirically derived constant (1.8×10^{-8} in the latest version of Rosenkranz (1998)), $x_{continuum}$ is the temperature exponent of the continuum (7.5 in the latest version of Rosenkranz (1998)), f is the frequency in GHz, C'_w is an additional empirically derived constant along with empirically derived $n_{continuum}$ and $x'_{continuum}$. The second term does not appear in Rosenkranz (1998), however, it was necessary to fit pure water vapor data with pressures exceeding 2 bars. The foreign gas contribution is defined as

$$\alpha_{c,f} = C_f P_{f,ideal} P_{H_2O,ideal}\theta^3 f^2 \ (\mathrm{km}^{-1}), \tag{42}$$

where C_f is an empirically derived constant (5.43×10^{-10} in the latest version of Rosenkranz (1998)). In the new jovian model C_f is derived in two parts one derived with respect to H_2 and the other due to He. This results in a modified value for $\alpha_{c,f}$ defined as

$$\alpha_{c,f} = C_{H_2} P_{ideal,H_2} P_{H_2O,ideal}\theta^3 f^2 + C_{He} P_{ideal,He} P_{H_2O,ideal}\theta^3 f^2 \ (\mathrm{km}^{-1}), \tag{43}$$

where C_{H_2} and C_{He} are empirically derived constants based upon our measurements. The total absorption due to water vapor is then written as

$$\alpha_{H_2O} = 4.342945(\alpha_{lines} + \alpha_{continuum}) \ (\mathrm{dB/km}), \tag{44}$$

with the necessary empirically derived constants summarized in Table 6. The factor 4.342945 is simply a conversion factor from units of km^{-1} to dB/km, where 1 optical depth $\mathrm{km}^{-1} = 10\log_{10}(e) \approx 4.342945$ (Please note that the number of digits extending past the decimal point are not an indication of the precision of the overall equation).

9. Data fitting process

This new model for the opacity of water vapor under jovian conditions was derived from an extensive laboratory measurement data set. The data set used to derive the opacity model was only a subset of the complete body of data taken. The three primary reasons for omitting data points for the model fit were: spread in data points at lower frequency resonances due to the limited sensitivity, possible preferential venting of H_2/He when taking measurements while decreasing pressure in the system (data taken after the maximum pressure was reached), and the elimination of experiment 17 owing to scatter in its data points and its limited value in a model for a jovian atmosphere. The spread in data points at lower frequency resonances arose primarily due to the low opacity values when smaller quantities of water vapor were measured. When opacity values approached the sensitivity threshold of 10^{-2} dB/km for the ~1.5 GHz and ~1.8 GHz resonances, quite a bit of scatter was observed. Once the compromised data points had been omitted, the process of fitting the data points began with the pure water vapor data set, or the first pressure in experiments 1–16. The method used a Levenberg–Marquardt optimization technique with a minimization function of

Table 6
Empirically derived constants for the new H_2O water vapor model.

C_w	$4.36510480961 \times 10^{-7}$
C'_w	$2.10003048186 \times 10^{-26}$
$x_{continuum}$	13.3619799812
$n_{continuum}$	6.76418487001
$x'_{continuum}$	0.0435525417274
C_{H_2}	$5.07722009423 \times 10^{-11}$
C_{He}	$1.03562010226 \times 10^{-10}$

$$\chi^2 = \frac{(s \times (\alpha_{meas} - \alpha_{model}))^2}{Err^2_{\alpha,meas}}, \tag{45}$$

where s is an adjustable scale factor, α_{meas} is the measured absorption coefficient, α_{model} is the absorption coefficient for the model undergoing optimization, and $Err_{\alpha,meas}$ is the measurement error for the measured absorption coefficient. Note that when fitting a model, effects of uncertainty of the environmental conditions Err_{cond}, must also be added to the absorptivity data. The conditional uncertainties to be added to our absorptivity data were initially estimated by applying the uncertainties in temperature, pressure, mixing ratio and compressibility to the Goodman and DeBoer models. Since the resulting uncertainties were insignificant (see Hanley, 2008), the new model was fit directly to the absorptivity data. Once the new model was developed, the effects of conditional uncertainties on the new model's performance were computed and are discussed below in Section 10. The scale factor s was adjusted so as to maintain the relative contribution of the lower precision data taken at 375 K when fitting the model so as to develop an accurate

Please cite this article in press as: Karpowicz, B.M., Steffes, P.G. In search of water vapor on Jupiter: Laboratory measurements of the microwave properties of water vapor under simulated jovian conditions. Icarus (2011), doi:10.1016/j.icarus.2010.11.035

temperature dependence in the model. The value of s was set to 10 for experiments 1–6, and a value of unity for all other experiments. The pure water data set was initially fit without the C'_w in Eq. (41), however, experiments 9 and 11 fit poorly due to the large amount of water vapor. The C'_w term was added and optimized adjusting values of s for experiments 9 and 11 such that they would be weighted more than data points with less opacity. The inclusion of the C'_w term significantly improved the fit for experiments 9 and 11 without compromising the quality of fit for the remaining experiments. Once the pure water vapor data set was fit, the values for C_{He} were fit using data taken with a mixture of H_2O and Helium only. This involved the second pressure in experiments 5, 10, 12, 13, 15, and 16. Next, the data set using a mixture of hydrogen and water vapor was used to optimize C_{H_2} using all data in experiments 6, 11, and 14. Finally C_{He} and C_{H2} were optimized together using all experiments from 1 to 16.

10. Model performance

The optimized model performed quite well when considering the relatively low level of opacity observed in these experiments. The results from all experiments superimposed over the new model (black, solid line), DeBoer (1995) (described in de Pater et al. (2005)) (blue, dotted line), and Goodman (1969) (red, dashed line) are shown in Figs. 4–7. The model reproduces the data set quite well, and as shown in Table 7, the model results lie within the 2σ error bars of the measurement for 720 out of a total of 929 fitted data points. The model performance surpasses any previously-used jovian water vapor opacity model, and the use of either the DeBoer (1995) (described in de Pater et al. (2005)) or Goodman (1969) models should be discontinued. For reference, the dashed lines in Figs. 4–6, represent the conditional errors (Err_{cond}) propagated through each water vapor absorption model. The propagated error due to conditional uncertainties is greater for our model, owing to its enhanced sensitivity to the presence of water vapor. Both the (DeBoer, 1995) (described in de Pater et al. (2005)) and the Goodman (1969) models have unrealistically high values for foreign gas broadening, and insufficiently low dependence for self broadening effects.

11. Discussion

The primary objective of this work has been to derive a centimeter-wave opacity model for water vapor under deep jovian conditions. The water vapor opacity model is based upon extensive laboratory measurements conducted under temperatures ranging from 375 to 525 K and pressures up to 100 bars. The model developed provides a good fit with experimental data, and is the first centimeter-wave opacity model developed for water vapor under jovian conditions to be based on laboratory experiments. When compared with the model for water vapor opacity (Goodman, 1969) used by Janssen et al. (2005) or the DeBoer model described in de Pater et al. (2005), several differences are noteworthy. First, for mixtures with larger abundances of water vapor (Figs. 4 and 5), the Goodman model dramatically understates the microwave opacity from the water vapor, largely because it makes no allowance for the effects of self-broadening, which is an enormous effect. While, the DeBoer model appears reasonably accurate at moderate pressures and relatively large water vapor abundances, it appears to overstate the opacity at higher pressures since it uses only line structure to compute opacity, and has no continuum component in the absorption model. The lack of a continuum component and the lack of inclusion of the effects of compressibility also explain why the Goodman model fits well at some higher pressure–temperature points, but not all data points (see Fig. 6).

The effects of the new model on jovian microwave emission are currently under study and will be presented in a future paper. However, preliminary radiative transfer studies with the new model for water vapor opacity indicate up to a 5% increase of the 30-cm limb darkening reported by Janssen et al. (2005) for an atmosphere with elevated (super-solar) water vapor abundance.

Finally, since the model developed was based on laboratory measurements taken over a limited range of temperatures and pressures (375–525 K and pressures up to 100 bars), caution

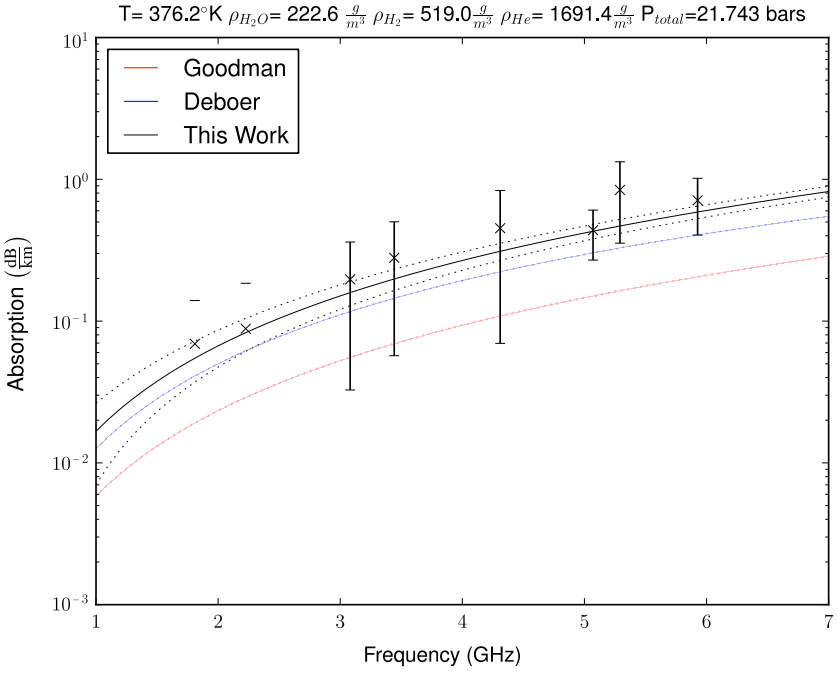

Fig. 4. Experiment 4 with H_2/He mixture 21.7 bars total pressure. Dotted lines represent errors in measurement conditions propagated through each absorption model.

Please cite this article in press as: Karpowicz, B.M., Steffes, P.G. In search of water vapor on Jupiter: Laboratory measurements of the microwave properties of water vapor under simulated jovian conditions. Icarus (2011), doi:10.1016/j.icarus.2010.11.035

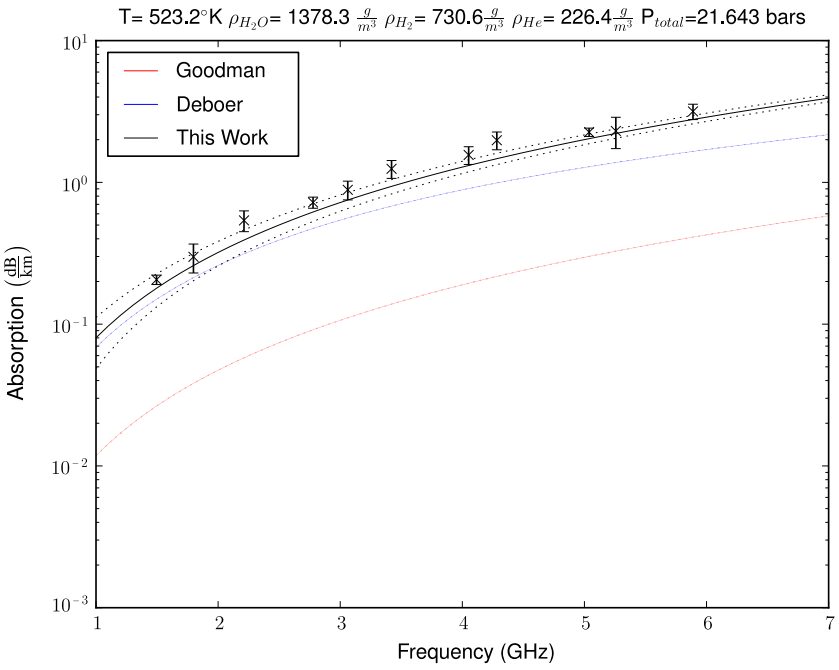

Fig. 5. Experiment 9 with Factory H_2/He mixture 21.6 bars total pressure. Dotted lines represent errors in measurement conditions propagated through each absorption model.

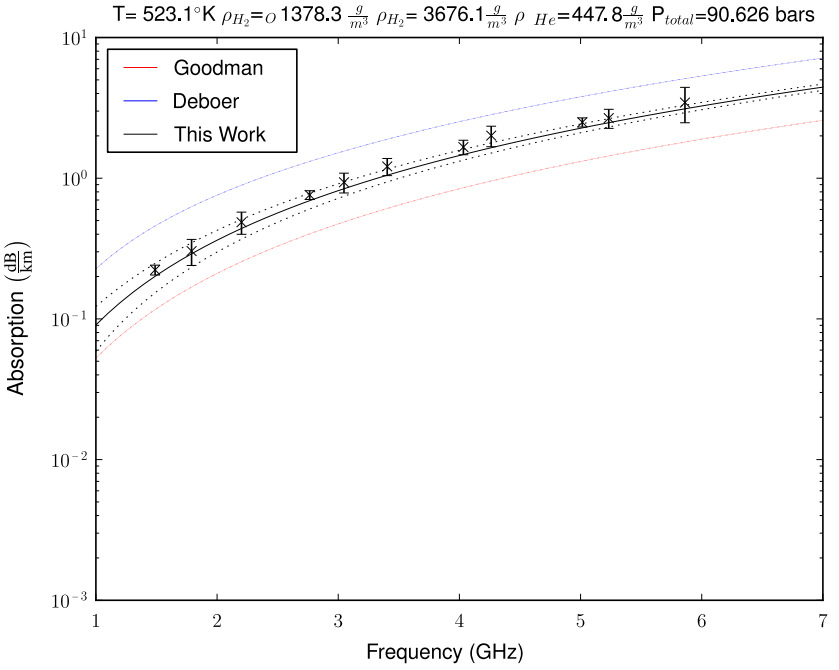

Fig. 6. Experiment 9 with H_2/He mixture 90.6 bars total pressure. Dotted lines represent errors in measurement conditions propagated through each absorption model.

should be exercised when applying the model to the much higher pressures and temperatures characteristically sensed at longer wavelengths. There is no evidence that the model presented will remain valid at temperatures exceeding one thousand degrees or pressures exceeding five hundred bars.

12. Conclusions

Nearly 2000 laboratory measurements of the microwave opacity of H_2O vapor in a H_2/He atmosphere have been conducted in the 5–21 cm wavelength range (1.4–6 GHz) at pressures from 30 mbars to 101 bars and at temperatures from 330 to 525 K. The mole fraction of H_2O (at maximum pressure) ranged from 0.19% to 3.6% with some additional measurements of pure H_2O. These results have enabled development of the first model for the opacity of gaseous H_2O in a H_2/He atmosphere under jovian conditions developed from laboratory data. The new model is based on a terrestrial model of Rosenkranz (1998), with substantial modifications to reflect the effects of jovian conditions. The new model for water vapor opacity dramatically outperforms previous models.

Please cite this article in press as: Karpowicz, B.M., Steffes, P.G. In search of water vapor on Jupiter: Laboratory measurements of the microwave properties of water vapor under simulated jovian conditions. Icarus (2011), doi:10.1016/j.icarus.2010.11.035

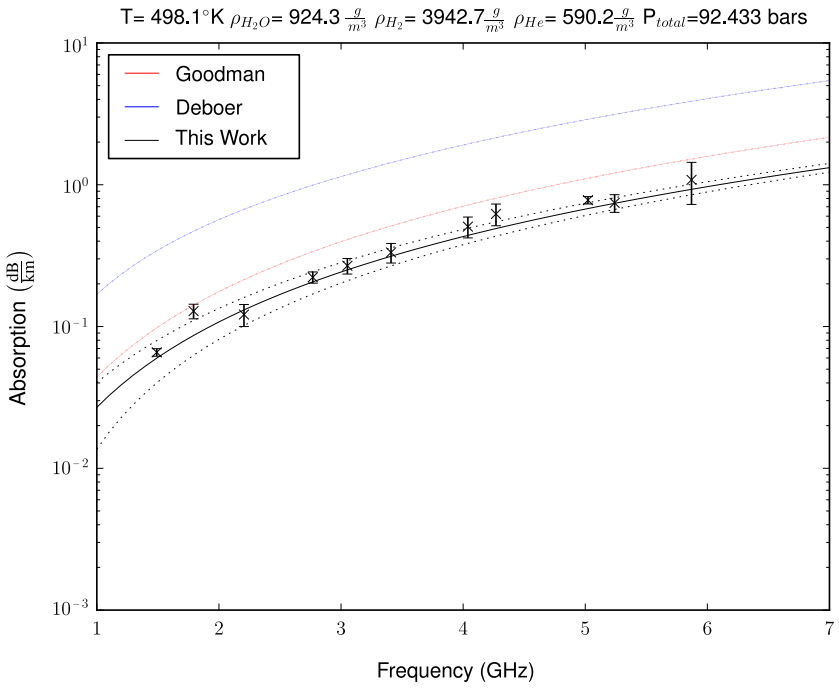

Fig. 7. Experiment 13 with H_2/He mixture 92.4 bars total pressure. Dotted lines represent errors in measurement conditions propagated through each absorption model.

Table 7
Performance of the model in the current work versus existing jovian opacity models.

Model	Data points within 2σ (counts)	Maximum deviation (dB/km)	Minimum deviation (dB/km)	Mean deviation (dB/km)
This work	720	0.8321	1.1110×10^{-6}	0.0782
DeBoer (1995)	312	2.940	4.7978×10^{-5}	0.3382
Goodman (1969)	402	2.907	1.2945×10^{-4}	0.2148
Total	929.0			

These results will help quantify the sensitivity of microwave radiometric studies of Jupiter to the abundance of atmospheric water vapor (de Pater et al., 2005; Janssen et al., 2005), as well as provide a clearer understanding of the role deep atmospheric water vapor may play in the decimeter-wavelength spectrum of Saturn. Future work will include development of a new equation-of-state for the jovian atmosphere based on the measurements of the compressibility of the gas mixtures conducted during these experiments. Additionally, future radiative transfer studies will reflect the effect of using the new formalism on retrieval sensitivity for water vapor from the Juno Microwave Radiometer (MWR). Finally, the new high-pressure laboratory system described in this paper will be used for measurements of the 1.4–6 GHz opacity of ammonia in an H_2/He atmosphere in the 7–94 bar pressure range. These measurements will be used to verify the applicability of the model developed by Hanley et al. (2009) (which was developed from measurements in the 0.1–12 bar pressure range) at much higher pressures.

Acknowledgments

The authors wish to acknowledge the invaluable help and assistance of Dr. Thomas Hanley (JHU-APL) and Ms. Kiruthika Devaraj (Georgia Tech). We are especially indebted to the Juno Microwave Radiometer (Juno-MWR) team for their input and review of our work. This work was supported by NASA Contract NNM06AA75C from the Marshall Space Flight Center supporting the Juno Mission Science Team, under Subcontract 699054X from the Southwest Research Institute.

References

Bleaney, B., Loubser, J.H.N., 1950. The inversion spectra of NH_3, CH_3Cl and CH_3Br at high pressures. Proc. Phys. Soc.: Sec. A 63, 483–493.
DeBoer, D.R., 1995. The microwave opacity of H_2S with applications to the tropospheric vertical structure of the jovian planets. Ph.D. Thesis, Georgia Institute of Technology.
DeBoer, D.R., Steffes, P.G., 1996. The Georgia Tech high sensitivity microwave measurement system. Astrophys. Space Sci. 236, 111–124.
de Pater, I., Deboer, D., Marley, M., Freedman, R., Young, R., 2005. Retrieval of water in Jupiter's deep atmosphere using microwave spectra of its brightness temperature. Icarus 173 (2), 425–447.
Fahd, A.K., 1992. Study and interpretation of the millimeter-wave spectrum of venus. Ph.D. Thesis, Georgia Institute of Technology, Atlanta.
Goodman, G.C., 1969. Models of Jupiter's atmosphere. Ph.D. Thesis, University of Illinois.
Hanley, T.R., 2008. The microwave opacity of ammonia and water vapor: Application to remote sensing of the atmosphere of Jupiter. Ph.D. Thesis, Georgia Institute of Technology.
Hanley, T.R., Steffes, P.G., 2007. A high-sensitivity laboratory system for measuring the microwave properties of gases under simulated conditions for planetary atmospheres. Radio Sci 42 (6), 1–12. No. RS6010.
Hanley, T.R., Steffes, P.G., Karpowicz, B.M., 2009. A new model of the hydrogen and helium broadened microwave opacity of ammonia based on extensive laboratory measurements. Icarus 202, 316–335.
Ho, W., Kaufman, I.A., Thaddeus, P., 1966. Laboratory measurement of microwave absorption in models of the atmosphere of Venus. J. Geophys. Res. 71 (21), 5091–5108.
Hoffman, J.P., Steffes, P.G., 2001. Laboratory measurements of the microwave opacity of phosphine: Opacity formalism and application to the atmospheres of the outer planets. Icarus 152, 172–184.
Janssen, M.A., Hofstadter, M.D., Gulkis, S., Ingersoll, A.P., Allison, M., Bolton, S.J., Levin, S.M., Kamp, L.W., 2005. Microwave remote sensing of Jupiter's atmosphere from an orbiting spacecraft. Icarus 173 (2), 447–453.
Joiner, J., Steffes, P.G., 1991. Modeling of Jupiter's millimeter wave emission utilizing laboratory measurements of ammonia (NH_3) opacity. J. Geophys. Res. 96, 17463–17470.

Please cite this article in press as: Karpowicz, B.M., Steffes, P.G. In search of water vapor on Jupiter: Laboratory measurements of the microwave properties of water vapor under simulated jovian conditions. Icarus (2011), doi:10.1016/j.icarus.2010.11.035

Karpowicz, B.M., 2010. In search of water vapor on Jupiter: Laboratory measurements of the microwave properties of water vapor and simulations of Jupiter's microwave emission in support of the Juno mission. Ph.D. Thesis, Georgia Institute of Technology.

Leachman, J., 2007. Fundamental equations of state for parahydrogen, normal hydrogen, and orthohydrogen. Master's thesis, University of Idaho.

Matousek, S., 2005. The Juno new frontiers mission. Tech. Rep. IAC-05-A3.2.A.04, California Institute of Technology.

Matthaei, G.L., Young, L., Jones, E., 1980. Microwave Filters, Impedance Matching Networks and Coupling Structures. McGraw-Hill, New York.

McCarty, R.D., 1990. A new wide range equation of state for helium. Adv. Cryogenic Eng. 35, 1465–1475.

Mohammed, P.N., Steffes, P.G., 2003. Laboratory measurements of the ka-band (7.5 mm to 9.2 mm) opacity of phosphine (PH_3) and ammonia (NH_3) under simulated conditions for the Cassini–Saturn encounter. Icarus 166, 425–435.

Morris, E.C., Parsons, R.W., 1970. Microwave absorption by gas mixtures at pressures up to several hundred bars. Aus. J. Phys. 23, 335–349.

Payne, V.H., Delamere, J.S., Cady-Pereira, K.E., Gamache, R.R., Moncet, J.-L., Mlawer, E.J., Clough, S.A., 2008. Air-broadened half-widths of the 22- and 183-GHz water-vapor lines. IEEE Trans. Geosci. Rem. Sens. 46 (11), 3601–3617.

Payne, V., Mlawer, E., Cady-Pereira, K., Moncet, J., 2011. Water vapor continuum absorption in the microwave. IEEE Trans. Geosci. Rem. Sens., in press.

Pozar, D.M., 1998. Microwave Engineering, second ed. Wiley and Sons, New York.

Rabinovich, V.A., 1995. Moist Gases: Thermodynamic Properties. Begell House.

Rosenkranz, P.W., 1998. Water vapor microwave continuum absorption: A comparison of measurements and models. Radio Sci. 33, 919–928.

Rothman, L.S. et al., 2009. The HITRAN 2008 molecular spectroscopic database. J. Quant. Spectrosc. Radiat. Trans. 110, 533–572.

Seward, T.M., Franck, E.U., 1981. The system hydrogen–water up to 440 °C and 2500 bar pressure. Ber. Bunsenges. Phys. Chem. 85, 2–7.

Seward, T.M., Suleimenov, O.M., Franck, E.U., 2000. pVT data for binary H_2–H_2O mixtures in the homogeneous region to 450 °C and 2500 bar. In: Steam, Water, and Hydrothermal Systems: Physics and Chemistry Meeting the Needs of Industry: Proceedings of the 13th International Conference on the Properties of Water and Steam. NRC Research Press, pp. 104–109.

Tyler, G.L., Howard, H.T., 1969. Refractivity of carbon dioxide under simulated martian conditions. Radio Sci. 4, 899–904.

von Zahn, U., Hunten, D.M., Lehmacher, G., 1998. Helium in Jupiter's atmosphere: Results from the Galileo probe helium interferometer experiment. J. Geophys. Res. 103, 22815–22830.

Wagner, W., Pruß, A., 2002. The IAPWS formulation 1995 for the thermodynamic properties of ordinary water substance for general and scientific use. J. Phys. Chem. Ref. Data 387–535.

Please cite this article in press as: Karpowicz, B.M., Steffes, P.G. In search of water vapor on Jupiter: Laboratory measurements of the microwave properties of water vapor under simulated jovian conditions. Icarus (2011), doi:10.1016/j.icarus.2010.11.035